IOP Publishing Environ. Res. Lett. 17 (2022) 045026 https://doi.org/10.1088/1748-9326/ac5edd

ENVIRONMENTAL RESEARCH
LETTERS

OPEN ACCESS

RECEIVED
30 October 2021

REVISED
28 January 2022

ACCEPTED FOR PUBLICATION
17 March 2022

PUBLISHED
4 April 2022

LETTER

Sea ice-free corridors for large swell to reach Antarctic ice shelves

N J Teder[1,*], L G Bennetts[1], P A Reid[2,3] and R A Massom[3,4,5]

[1] University of Adelaide, Adelaide, South Australia, Australia
[2] Australian Bureau of Meteorology, Hobart, Tasmania, Australia
[3] Australian Antarctic Program Partnership, Hobart, Tasmania, Australia
[4] Australian Antarctic Division, Hobart, Tasmania, Australia
[5] Australian Centre for Excellence in Antarctic Sciences (ACEAS), Institute for Marine and Antarctic Studies, University of Tasmania, Hobart, Tasmania
[*] Author to whom any correspondence should be addressed.

E-mail: nathan.teder@adelaide.edu.au

Keywords: Antarctic ice shelves, ocean hindcast, swell-ice shelves interactions, sea ice-free corridors, sea ice concentration

Abstract

Sea ice can attenuate Southern Ocean swell before it reaches Antarctic ice shelves and imposes flexural stresses, which promote calving of outer ice-shelf margins and influence ice shelf stability. An algorithm is developed to identify sea ice-free corridors that connect the open Southern Ocean to Antarctic ice shelves from daily satellite sea ice concentration data between September 1979 and August 2019. Large swell in the corridors available to impact the ice shelves is extracted from spectral wave model hindcast data. For a selection of ice shelves around the Antarctic coastline, corridors are assessed in terms of duration and areal extent. The availability of large swell to impact certain ice shelves through the corridors is evaluated from spectral wave data for daily statistical properties and the number of large swell days per year. Results integrated over a large number of ice shelves are used to assess overall trends. Large variations are found between individual ice shelves for both corridors and available swell, with contrasting trends between the West and East Antarctic Ice Sheet. The findings indicate ice shelves likely to experience prolonged periods of appreciable outer margin flexure due to large swell action, such as the Fimbul, Shackleton and Ross Ice Shelves, which could exacerbate climate-driven weakening and decreasing buttressing capacity, with implications for sea-level rise.

1. Introduction

Loss or weakening of Antarctic ice shelves, which fringe 74% of the Antarctic grounded ice-sheet boundary [1], has the potential to push Antarctic Ice Sheet mass losses and associated sea level rise substantially beyond current projections [2, 3]. Without effective buttressing at the coastline from ice shelves [4, 5], the Antarctic Ice Sheet is vulnerable to runaway dynamic retreat [6–8]. Reduction of ice shelf buttressing is already dominating Antarctic Ice Sheet dynamic thinning via accelerated glacial outflow to the Southern Ocean [9] leading to an observed acceleration in grounded ice-mass loss over recent decades [10]. Further changes in ice shelves will play a large part in determining the future dynamic response of the Antarctic Ice Sheet to a warming climate [11]. However, current projections contain deep uncertainties as the controlling physical processes are poorly understood, which in turn, translates into substantial uncertainties in Antarctica's contribution to sea-level rise in coming decades [2].

Around much of the Antarctic coastline, ice shelf basal melting by warm ocean water incursions is driving an increasing reduction in buttressing capacity [9]. Moreover, the Antarctic Peninsula has been host to a series of catastrophic ice shelf disintegration events that removed large proportions of the shelves in only days or weeks—most notably, the Larsen A and B Ice Shelves in 1995 [12] and 2002 [13–15], respectively, and the Wilkins Ice Shelf in 1996 and 2008–2009 [16]. The disintegration events led to a two- to eight-fold increase glacial flow into the Southern Ocean from their respective glaciers [14, 15].

The Antarctic Peninsula is the most northerly reach of Antarctica and has experienced strong climate warming in the lead up to the 21st century [17, 18]. At the same time, the annual duration and

extent of sea-ice coverage off the western and north-eastern Peninsula have shown negative trends since 1979 [19, 20], in broad contrast to other Antarctic regions. The response of Antarctic sea ice to climate variability and change is characterised by complexities, regional variations and recent high interannual variability [21, 22], which is emphasised by the consecutive years of record highs (peaking in 2014) closely followed by record lows (from 2016) [20]. Contemporary models are unable to reproduce the observed behaviours of Antarctic sea ice accurately, resulting in low confidence in projections of future trends in Antarctic sea ice coverage [2, 23].

In the years leading up to the disintegration events, the Wilkins and Larsen Ice Shelves were subjected to prolonged periods without sea ice buffers [19, 24, 25] protecting them from storm-generated swell by attenuating wave energy over the distance travelled [26]. Large-amplitude swell generated in the open ocean were able to reach the ice shelves through sea ice-free corridors, and repeatedly subjected the rifted and crevassed outer margins of the shelves to flexural stresses [25]. Compelling evidence indicates the process eventually precipitated extensive outer-margin calving, which acted as a trigger mechanism for the disintegration of large ice shelf areas [25] already destabilised by surface flooding, hydrofracture, thinning and glaciological weaknesses [9, 14, 27–30].

Ocean wave-induced flexural vibrations have been measured on Antarctic ice shelves (and ice tongues), at frequencies ranging from swell to tsunami and infragravity waves, including two campaigns on the Ross Ice Shelf from 2004–2006 [31] and 2014–2016 [32]. For over four decades, evidence has accumulated that wave-induced flexural vibrations could promote ice shelf calving events [33], but with a focus on tsunami and infragravity waves [34, 35], as they are unimpeded by attenuation due to sea ice cover [36] and reflection by the shelf front [37, 38]. The link between disintegration events and large swell [25], along with earlier observational work linking swell to calving events [39] and more recent work linking swell to ice shelf 'ice-quakes' [40], combined with the increasing trend for extreme waves in the Southern Ocean [41], highlights the potential for swell modulated by sea ice to play an increasingly important role in the future stability of Antarctic ice shelves. Recent theoretical modelling advances support the ability of swell to impart damaging strains [42].

In this Letter, we address the variability and trends in sea ice-free corridors for ice shelves around the Antarctic coastline and the availability of large swell in the corridors, building on a new 'coastal exposure' metric for the entire Antarctic circumpolar coastline and associated analysis of change and variability in the extent and timing of coastal exposure around Antarctica [43]. Here, algorithms are developed to (a) identify sea ice-free corridors from daily satellite sea ice concentration data, using the coastal exposure algorithm [43] as a first step, and (b) identify large swell in the corridors with the potential to impact an ice shelf from spectral wave data. The algorithms are used to extend the study of swell corridors on the Antarctic Peninsula leading up to the disintegration events [25] to wider spatio-temporal occurrence of (and possible trends in) swell corridors around Antarctica. Results are given for a selection of key Antarctic ice shelves, including the Thwaites and Pine Island Ice Shelves that fringe rapidly thinning glaciers [10], the Totten Ice Shelf whose dynamics are linked to the presence of a sea ice buffer [44] and the Cook Ice Shelf that recently recorded an acceleration in ice velocity [45]. Results integrated over a larger number of ice shelves are also given, and large-scale corridor and large swell behaviours impinging on the West and East Antarctic Ice Sheet are compared.

2. Methods and data

2.1. Corridor algorithm

Detection and delineation of sea ice-free corridors are calculated based on sea ice concentrations from satellite passive microwave data (NIMBUS-7 SMMR and DMSP SSM/I-SSMIS, Version 1 [46]). The sea ice concentration data covers the satellite era period between 1 September 1979 and 31 August 2019 at a 25 km^2 resolution. The data is only available on alternative days until the 19th of August 1987, and daily thereafter. For consistency, the full dataset was made daily by interpolating between consecutive data points at each spatial location up to the 19 August 1987.

Grid cells along the Antarctic coastline (from the gfsc_25s.msk land mask) occupied by an ice shelf front (based on the MEaSUREs plugin for the Antarctic Mapping Toolbox [28, 47], with a 25–150 m varying resolution) that are exposed to the open ocean, are calculated using an adapted version of the coastal exposure algorithm [43]. For each daily record of sea ice concentration the algorithm is as follows. (i) Identify potentially exposed cells as those having at least one adjacent cell (directly north, south, east or west) in the ocean and away from the coastline with a sea ice concentration $\leqslant c_{\min}$, where $c_{\min} = 15\%$ following the standard sea ice concentration threshold [46]. (ii) Consider each potentially exposed cell in turn. (ii.a) If either of the adjacent coastal cells has already been classified as being exposed for that day, the cell is then classified as exposed. (ii.b) If not, determine if the cell is enclosed in a polynya by checking the total connected area of non-coastal ocean cells with sea ice concentration $\leqslant c_{\min}$, and if the area is $\geqslant A_{\exp}$ $(=5\times10^6 km^2)$ identify the cell as exposed. (iii) Terminate the algorithm when all cells have been classified.

Sea ice-free corridors are then calculated using the following steps: (i) Group exposed cells on the coastline occupied by an ice shelf front. (ii) Choose an ice shelf from the 69 considered in this study (covering >99% of total ice shelf area). (iii) Choose an exposed cell on the coastline for the chosen shelf. (iv) Calculate the straight line (with respect to north–south vs. east–west space) between the northwestern corner of the exposed coastline cell and the northwestern corner of a chosen cell on the northern most boundary of the sea ice data (≈42° S). (v) Find one cell per discrete latitude intersected by the straight line, arbitrarily choosing the eastern-most cell if the straight line intersects more than two cells at a given latitude. (vi) Moving north from the coastal cell, identify the cells from (v) as being in the corridor for the chosen shelf if they are not land cells (including coastal cells) and have sea ice concentration $\leqslant c_{\min}$. (vii) Terminate (vi) once a land cell (not including coastal cells) or a cell with sea ice concentration of $>c_{\min}$ is found. (viii) Repeat (v)–(vi) for all cells at the northernmost boundary of the sea ice concentration data. (ix) Repeat (iii)–(viii) for all exposed cells on the coastline for the chosen shelf. (x) Identify the union of all corridor cells found from (iii)–(ix) as the corridor for the chosen shelf. (xi) Repeat for all 69 ice shelves. Corridors are analysed up to the maximum northern extent of sea ice off the Antarctic coastline or 57.5° S, depending on which is farther south on that particular day, as the cut-off is to prevent sea ice around South Georgia Island from influencing corridor areas.

Two distinct types of corridor form. One is where the corridor occupies a simply connected region of the open ocean (sea ice concentration $\leqslant c_{\min}$), which is directly offshore from the ice shelf (figure 1(a)). The other is where a corridor is interrupted by the presence of islands or, in the example shown in figure 1(b), icebergs. Choosing $A_{\exp} = 5 \times 10^6$ km^2 prevents corridors from being identified in polynyas (e.g. figure 1(c)), under the assumption that large amplitude swells will generally not be generated in the polynyas or penetrate into the polynyas from the open (ice-free) Southern Ocean to the north.

2.2. Swell

Wave properties in the corridors are extracted from a WAVEWATCH III model hindcast (CAWCR Wave Hindcast, Aggregated Collection [48]), with main interest in the significant wave height (H_S) as a proxy for wave energy. The wave data is at 0.4° resolution and hourly frequency from 1 January 1979 onwards. Sea ice concentration in WAVEWATCH III is incorporated using the CFSR dataset [49]. Following Tolman [50], waves are unaffected by sea ice concentrations $\leqslant$25% and waves are shut-off for concentrations $\geqslant$75%. For concentrations between 25% and 75%, wave amplitudes are reduced as if sub-grid scale islands were present. The latest WAVEWATCH III developments in modelling wave propagation through the sea-ice covered ocean [51] are not incorporated in the hindcast (or any other wave hindcast to our knowledge).

The largest wave that may impact a certain shelf on a particular day is determined using the following algorithm. For a chosen shelf and day: (a) Identify all cells in the wave hindcast in the corridor for the chosen shelf on the chosen day, allowing for only part of a cell to occupy the corridor. (b) For each daily record on the chosen day in the hindcast, filter the wave data in the corridor cells to only those for which the mean wave direction has a southerly component and is not obstructed by the coastline surrounding the shelf (i.e. if the shelf is in a bay). (c) From the remaining data, retain only the maximum significant wave height, $H_S^{\max}$.

3. Results and discussion

3.1. Sea ice-free corridors

Figures 2(a)–(l) shows a 40-year time-series of yearly corridor properties for a selection of twelve major ice shelves around the Antarctic coastline. Years are taken as starting from September, when sea ice extent peaks [20] through to August the following year. Corridors are evaluated in terms of the fraction of days they exist in each year (D_{cor}; grey curves) and the maximum yearly corridor area normalised by the potential maximum corridor area ($A_{\text{cor}}^{\max}$; i.e. without sea ice so the corridors are constrained only by the coastline).

On the southwestern Antarctic Peninsula, the Wilkins Ice Shelf (figure 2(a)) has an average $D_{\text{cor}} = 0.23$ (85 days a year), which is the largest value for the West Antarctic Ice Sheet. A peak of $D_{\text{cor}} = 0.57$ (208 days) occurred during September 2007 to August 2008 coinciding with multiple partial disintegration events between February and July 2008 [16], consistent with observations of reduced sea ice coverage and duration offshore over that period [25]. Of some note is a regime change that occured between the first nine years, when the mean $D_{\text{cor}} = 0.08$ and $A_{\text{cor}}^{\max} = 0.22$ are relatively small, and the subsequent 31 years, when the mean $D_{\text{cor}} = 0.28$ and $A_{\text{cor}}^{\max} = 0.57$ are much greater.

On the southeastern Antarctic Peninsula, the Larsen C Ice Shelf (figure 2(b)) had no corridors for 28 of the 40 years, and corridors appearing for only a small fraction of days ($D_{\text{cor}} < 0.05$) for 34 years. The absence of corridors is caused by typical presence of perennial sea ice that survives throughout summer in the western Weddell Sea [52, 53]. The results are a proxy for the Larsen A and B Ice Shelves (indicated on the figure 2 map), although the Larsen C Ice Shelf tends to have less frequent and relatively smaller corridors than the more northerly shelves. The Larsen C Ice Shelf experienced its most frequent and largest corridors ($D_{\text{cor}} = 0.38$ and $A_{\text{cor}}^{\max} = 0.55$) in the 2001–02 season, coinciding with the onset of the Larsen B Ice Shelf disintegration [14, 15].

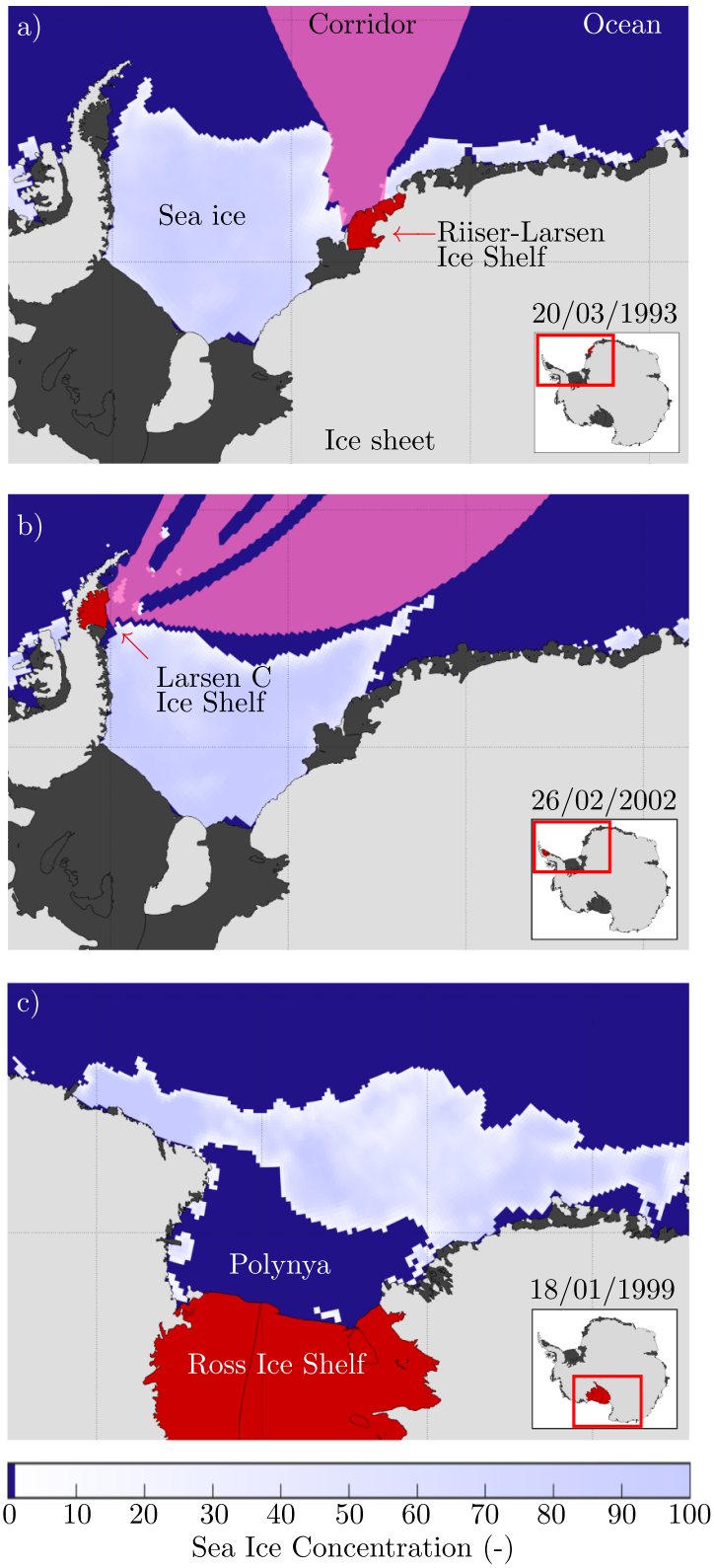

Figure 1. (a) and (b) Two typical sea ice-free corridors: (a) occupying simply connected region to the open ocean (example is the Riiser–Larsen Ice Shelf on the 20 March 1993); (b) where icebergs create gaps in the corridor (example is the Larsen C Ice Shelf on the 26 February 2002). Note that in the example shown, one side of the corridor is bounded by land rather than sea ice. (c) Polynya identified by the algorithm for which corridors are not assigned (example is the Ross Ice Shelf on the 18 December 1999). Straight lines appear curved due to the projection used (Lambert Azimuthal Equal-Area Projection).

Sea ice-free corridors typically exist each year for ice shelves in the eastern Weddell Sea (Brunt and Fimbul; figures 2(c) and (d)), in the Indian Ocean (Amery; figure 2(f) and western Western Pacific Ocean (Shackleton; figure 2(h) sectors, where the mean D_{cor} ranges from 0.13 for the Brunt Ice Shelf to 0.27 for the Fimbul Ice Shelf. They also have relatively large maximum corridor areas, with the

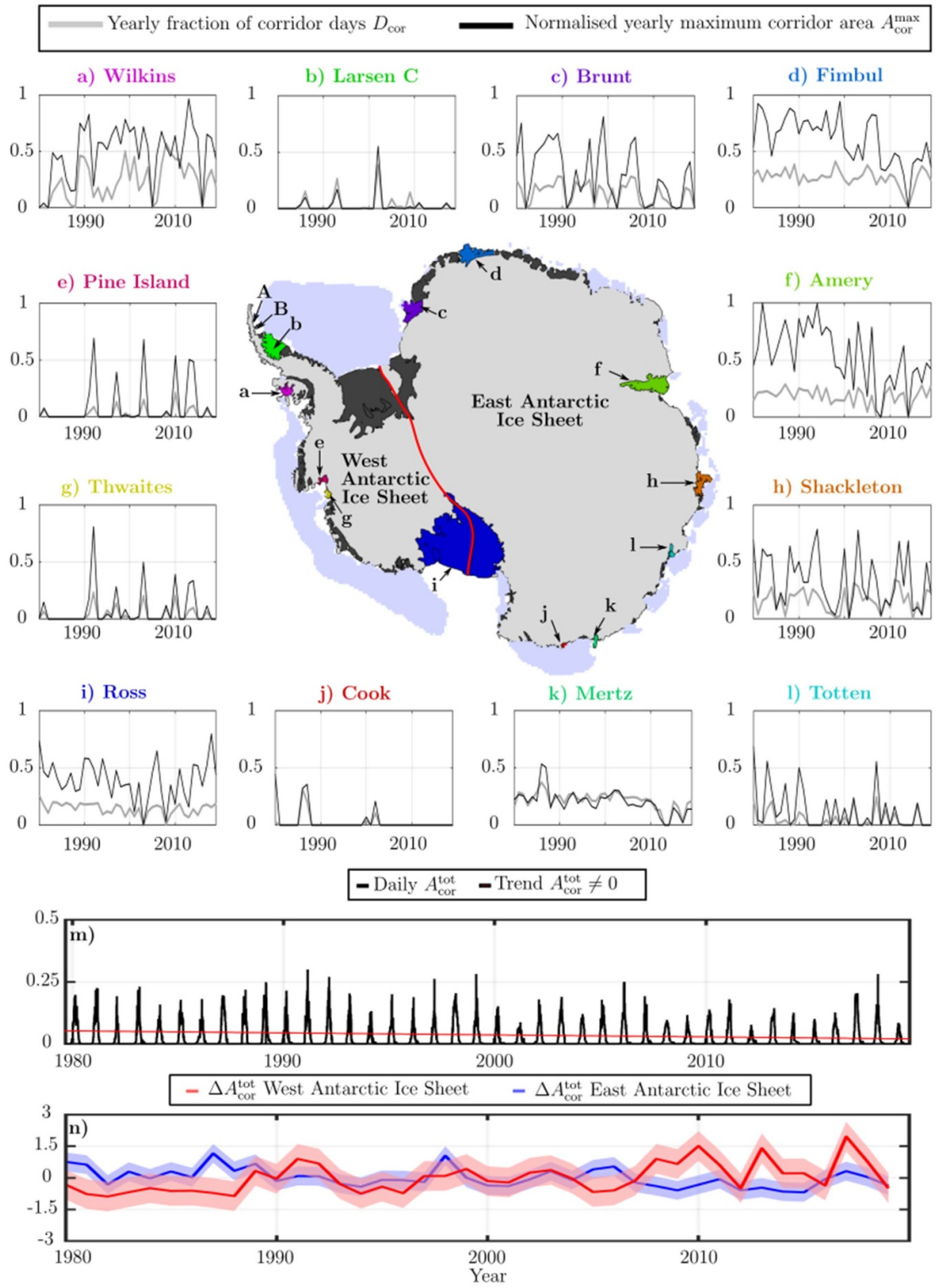

Figure 2. (a)–(l) Time-series of corridor properties for twelve major Antarctic shelves over the September–August yearly periods: fraction of exposed days per year (D_{cor}, grey lines); maximum corridor area over the year normalised by maximum potential corridor area (when no sea ice is present; A_{cor}^{max}, black lines). The shelves are marked on the map of Antarctica in the centre of the panels (colour-coded with panel titles). Other ice shelves are indicated (dark grey), along with the boundary between the West and East Antarctic Ice Sheet (red line). For reference, the former locations of the Larsen A and B Ice shelves are also marked (A and B, respectively). Areas of the Southern Ocean that have $\geqslant$80% of days in the Austral summer and autumn with a sea ice concentration $\geqslant c_{min}$ are shaded in blue, which indicates the areas that corridors are least likely to occur. (m) Daily total corridor area for all shelves normalised by total potential area (A_{cor}^{tot}; black line), and the trend line for days when corridors exist (red line). (n) Variation of total yearly A_{cor}^{tot} for ice shelves on the East Antarctic Ice Sheet (blue line) and West Antarctic Ice Sheet (including the Ross Ice Shelf; red line) from the mean values, with standard deviations indicated by shaded areas.

Fimbul Ice Shelf consistently the largest, closely followed by the Amery Ice Shelf (mean $A_{\mathrm{cor}}^{\mathrm{max}} = 0.6$ and 0.53, respectively). The Brunt and Fimbul Ice Shelves have decreasing trends for D_{cor} and $A_{\mathrm{cor}}^{\mathrm{max}}$ over the 40 years, with corridors decreasing by roughly one day a year. This is in line with decreasing coastal exposure in the Weddell Sea sector [43]. The Amery Ice Shelf also has a decreasing D_{cor} trend but only by roughly half a day a year, and the Shackleton Ice Shelf has no trend.

East of the Shackleton Ice Shelf, the Totten Ice Shelf (figure 2(l)) has been thinning rapidly [28], with periods of accelerated thinning linked to regional sea ice thinning [44]. The local coastline supports fast-ice that breaks down in November–December and covers the bay in unconsolidated sea ice during January [44, 54], which creates highly variable corridor seasons. Corridors exist in half of the 40 years and with mean $D_{\mathrm{cor}} = 0.04$ and a mean $A_{\mathrm{cor}}^{\mathrm{max}} = 0.24$ in the years they exist.

At the eastern end of the Western Pacific Ocean sector, the Mertz and Cook Ice Shelves (figure 2(j) and (k)) have markedly different corridor properties to each other, despite being only about 350 km apart. The Mertz Ice Shelf, which juts into the ocean as an ice tongue, has corridors primarily located on its western side. Its corridor properties are consistent up to 2010–2011, when half the ice tongue calved [55]. Over the subsequent nine years, two years have no corridors and the mean $D_{\mathrm{cor}} = 0.12$ is half that over the first 31 years. The ice tongue traps sea ice on its eastern side [56], leading to the Cook Ice Shelf having corridors in only five years and none in the last 16 years, despite the major ice tongue calving and reduced sea ice production [57, 58]. The behaviour is likely linked to the presence of iceberg B–9B [57] and areas of small grounded icebergs that act as barriers to the westward advection of coastal sea ice in the Antarctic Coastal Current [56].

The ocean north of the Ross Ice Shelf (figure 2(i)) is characterised by the large and recurring Ross Sea polynya [59]. The polynya generally breaks open between late December–early March to create corridors for about 50 days a year ($D_{\mathrm{cor}} \approx 0.14$). The calving and subsequent grounding of the very large C–19 iceberg in 2002 created the only year without corridors, as it prevented the polynya from breaking open in the following Austral summer [60].

The appearance of corridors for the Thwaites Ice Shelf (figure 2(g)) is highly variable, however it follows the increasing coastal exposure trend in the Amundsen and Bellingshausen Sea sector [43]. There is a regime change between the first ten years, over which corridors only exist in one year, to the last 30 years, where corridors exist in just under half the years. Corridor formations were less frequent for the Pine Island Ice Shelf (figure 2(e)), largely due to the consistent formation of polynyas in Pine Island Bay [61] and the Thwaites Ice Tongue blocking incoming swell. The Thwaites Ice Tongue is retreating [62], making it likely that corridors will become more common for the Pine Island Ice Shelf in future years.

The presence of corridors is seasonal, as indicated by the daily ratio of the total area occupied by the corridors for each of the ice shelves to the total potential area ($A_{\mathrm{cor}}^{\mathrm{tot}}$; figure 2(m)), with the average corridor season from late December to mid-April. The season length has a positive trend of 0.39 ± 0.37 days a year over the 40 years.

The total normalised corridor area has a weak decreasing trend of $(8.1 \pm 1.1) \times 10^{-4}$ per year during the corridor seasons (i.e. when corridors exist; figure 2(m), red line), which is followed by a weak negative trend in the seasonal peaks. Ice shelves on the East Antarctic Ice Sheet have driven the weak decrease in total corridor area (figure 2(n), blue line), consistent with the decrease in coastal exposure length across East Antarctica [43]. In contrast, total corridor area for ice shelves on the West Antarctic Ice Sheet had increased over the 40 years (figure 2(n), red line).

3.2. Swell availability

The seasonality and strength of swell available to reach ice shelves through the sea ice-free corridors is illustrated by a climatology of daily maximum significant wave heights ($H_{\mathrm{S}}^{\mathrm{max}}$) for a selection of eight ice shelves (figure 3(a)). Seasons of available swell follow the corridor seasons, i.e. late December to mid-April on average. The maximum significant wave heights increase as corridors start appearing, reach their peaks when corridors are most frequent (in February–March), and then decrease as the corridors begin closing towards the winter shut-off.

The Wilkins Ice Shelf has the longest swell season, stretching from December into early July, and with mean $H_{\mathrm{S}}^{\mathrm{max}} > 4$ m from late February to early-May. On the other (eastern) side of the Antarctic Peninsula, the swell season for the Larsen C Ice Shelf starts earlier than the others in late October/early November and ends relatively early in late March, closely matching the weakening Riiser–Larsen Sea low pressure system in the Weddell Sea, which drives regional sea ice drift [63]. Daily mean maximum swell data for the Larsen C Ice Shelf only has a mean $H_{\mathrm{S}}^{\mathrm{max}}$ up to 0.4 m.

The Cook and Thwaites Ice Shelves also have swell seasons that end in late March/early April, which is earlier than the average. Mean $H_{\mathrm{S}}^{\mathrm{max}}$ values for the Cook Ice Shelf are of similar magnitude to those for the Larsen C Ice Shelf, but those for the Thwaites Ice Shelf are larger, e.g. typically >0.75 m from mid-February to early March. The Totten Ice Shelf has comparable available swell to the Thwaites Ice Shelf but with a larger and later peak.

By comparison, the Ross, Fimbul and Shackleton Ice Shelves have considerably larger available swell, comparable to the Wilkins Ice Shelf. The Fimbul and Shackleton seasons extend beyond the average to early

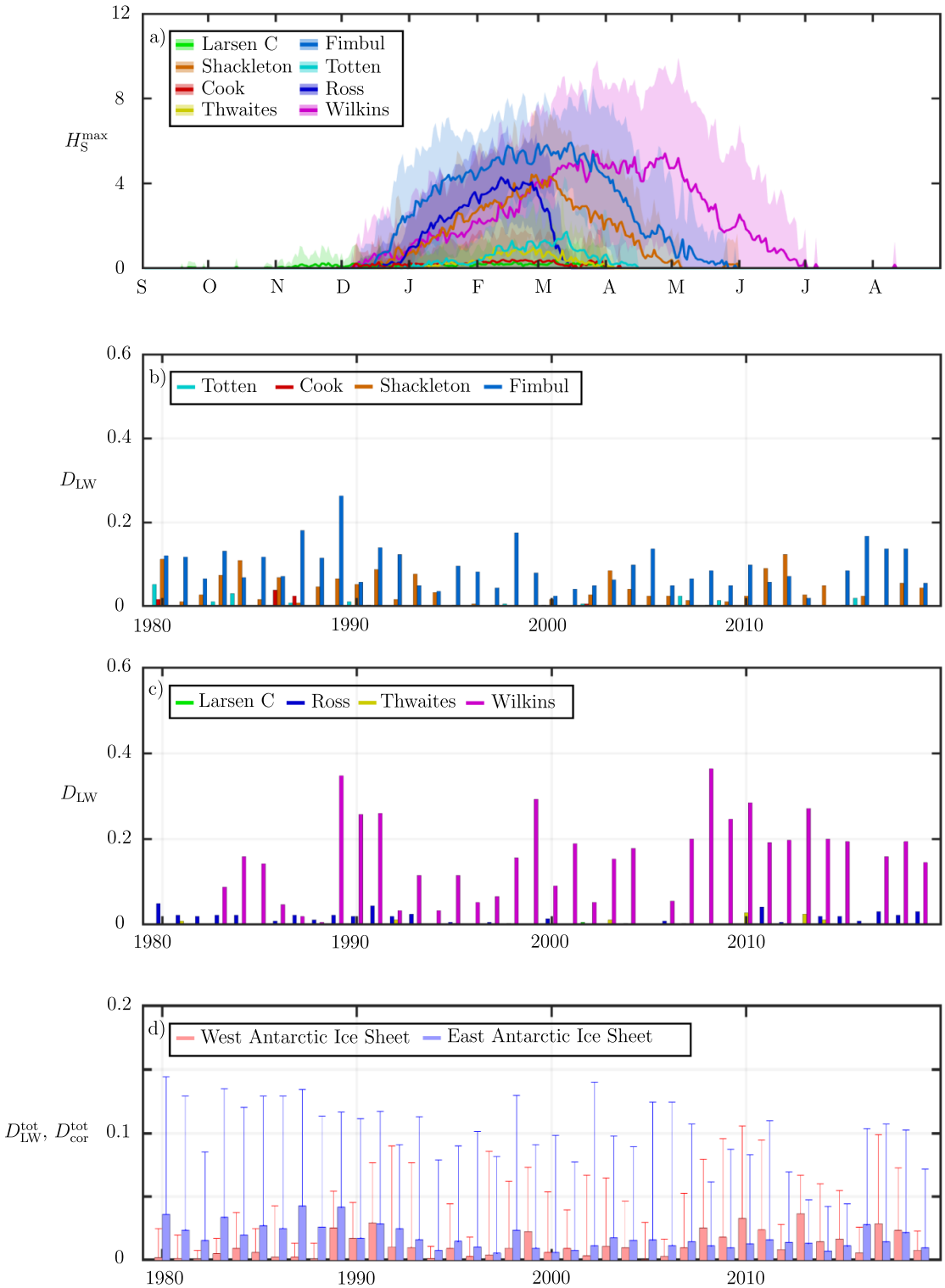

Figure 3. (a) Daily mean maximum significant wave height available in corridors for chosen ice shelves (lines) plus/minus one standard deviation (shaded areas). (b) and (c) Fraction of days in year (September through August) with large available swell ($H_S^{max} \geqslant 6$ m and denoted as D_{LW}) for chosen shelves on the (b) West and (c) East Antarctic Ice Sheet. (d) Mean fraction of days per year with large available swell per shelf over all shelves considered on West (red bars) and East (blue bars) Antarctic Ice Sheet, and corresponding mean fractions of days per year where corridors exist (whiskers).

May and late May, respectively, whereas the Ross Ice Shelf season ends abruptly in mid-March, when the Ross Sea polynya closes, consistent with seismic observations [31, 40].

The Wilkins Ice Shelf sea ice-free corridor has large swell, defined as $H_S^{max} > 6$ m [64], for $\geqslant$70 days a year in fourteen of the 40 years, and nine of the last twelve years. Large swell were available for approximately 133 days (0.35×365) from September 2007 to August 2008, coinciding with multiple partial disintegration events that occurred in 2008 [65].

The Fimbul Ice Shelf had large swell available for ⩾35 days a year for seventeen of the 40 years and ⩾50 days a year in eight years. There is an indication of a decreasing trend of large swell for the Fimbul Ice Shelf, e.g. the mean over the first twenty years is a factor 1.4 larger than the mean over the last twenty years, although three of the final four years have ⩾50 days of large swell available. The Shackleton Ice Shelf has large swell available for over 18 days a year for five of the 40 years, and a mean for the first twenty years a factor 1.2 greater than the mean in the last twenty years.

The Ross Ice Shelf has large available swell for 28 out of the 40 years, with large waves for seven days a year on average. Sea ice-free corridors with large swell available occurred during the seismic observations from November 2004 to May 2006 [31], but the average over this period was only two days a year, i.e. under a third of the expected number. Corridors with large swell available are more frequent during the seismic observations from October 2014 to November 2016 [40], particularly for the 2015–2016 season (seven days).

The Thwaites Ice Shelf has available large swell in only eight of the 40 years. In those years for which large swells are available, they occur for over five days a year on average, and three of the last ten years have large swell available. The Larsen C and Cook Ice Shelves have large swell available in only one and four years, respectively. Large swell has only been available to the Larsen C Ice Shelf for a total of two days over the 40 years. The Cook Ice Shelf has large swell for eight days a year on average in the four years it has availability, but it experienced no large swell in the last seventeen years up to 2019.

The large swell available for ice shelves on the West and East Antarctic Ice Sheet has contrasting trends over the 40-year record (figure 3(d) bars). During the first ten years, an ice shelf on the East Antarctic Ice Sheet has large swell available on average for eleven days a year, which far outweighs the two days a year on the West Antarctic Ice Sheet. For the subsequent twenty years, the East and West Antarctic Ice Sheet are closer to parity, with large swell available for approximately five and four days a year, respectively. Over the last ten years, the West Antarctic Ice Sheet has large swell available for seven days a year, which outweighs the five days a year for the East Antarctic Ice Sheet.

The ratio of days with large available swell (figure 3(d) bars) to days with sea ice-free corridors (shown as whiskers) has decreased for ice shelves on the East Antarctic Ice Sheet but increased on the West Antarctic Ice Sheet. Therefore, the trends in large swell available on the East and West Antarctic Ice Sheet are not solely determined by the number of corridor days, and are likely to also be influenced by trends in both corridor area and waves.

4. Concluding remarks

We conducted the first analysis of sea ice-free corridors connected to Antarctic ice shelves and available large swell in the corridors with the potential to impact the ice shelves, by applying new algorithms to daily sea ice concentrations from passive microwave data and hourly wave spectra from a model hindcast, from the 1st of September 1979 through to the 31st of August 2019. The analysis was applied to a selection of major ice shelves around the Antarctic coastline. The average corridor season lasts from late December to mid-April, but the number of days a year corridors exist and the areas they occupy were found to depend strongly on local characteristics of both the coastline and sea ice, including polynyas (Ross and Pine Island Ice Shelves), the presence and breakout of fast ice (Totten Ice Shelf) the presence of perennial sea ice offshore (Larsen C Ice Shelf) and the effect of ice tongues and grounded icebergs in maintaining regional near-shore sea-ice coverage (Mertz and Pine Island Ice Shelves). Evidence was found that trends in corridor properties follow trends in sea ice extent, particularly negative corridor trends for ice shelves in the Weddell Sea sector reflecting the positive trends in sea ice coverage and extent. Large swell availability also varies considerably between shelves, ranging from only one days over 40 years (Larsen C Ice Shelf) to tens of days in a year for multiple years (Wilkins, Fimbul, Shackleton, Ross and Thwaites Ice Shelves).

The results were integrated over 69 ice shelves to assess overall large-scale trends and compare behaviours on the West and East Antarctic Ice Sheet. Corridor season lengths were found to have a weak increasing trend and total corridor areas a weak decreasing trend driven by ice shelves on the East Antarctic Ice Sheet that outweighs an increasing trend on the West Antarctic Ice Sheet. Ice shelves skirting the West and East Antarctic Ice Sheet also showed opposing trends in total days of available large swell a year, with an increasing trend for the west and a decreasing trend for the east.

The corridor and swell algorithms have been designed for use with different sea ice and wave products and at different resolutions. Therefore, the study could be extended to test the corridor properties using different sea ice concentration data (e.g. the NSIDC Climate Data Record from Passive Microwave Sea Ice Concentration [66]) and the large available swell using different spectral wave data (e.g. the ERA5 based ocean wave hindcast [67]). Moreover, the accuracy of individual corridor predictions could be assessed by applying the corridor algorithm to sea ice concentration information extracted from cloud-free MODIS visible and thermal satellite imagery (e.g. at 250 m resolution following [68]).

The algorithms could potentially also be applied to climate model outputs to generate projections of

corridors and available swell for ice-shelf modelling purposes. For example, the corridor algorithm could be applied to sea ice concentration data from models that contribute to the latest phase of the Coupled Model Intercomparison Project (CMIP6), which typically give daily projections up to 2100 at approximately one degree spatial grid [69, 70] i.e. coarser resolutions than in the present study. The available swell algorithm could then be applied to projections of waves generated using WAVEWATCH III and forced by the CMIP6 model outputs [71, 72]. Impacts of ocean waves on sea ice are being integrated into the latest versions of sea ice models, such as CICE [73] and LIM3 [74], which may promote direct incorporation of ocean wave models in future CMIP phases and provide more accurate swell data in sea ice-free corridors for extended studies.

Data availability statement

The data and code used in this study are freely available through the Australian Antarctic Data Centre at the following DOI: https://doi.org/10.26179/jk2f-bv91.

Acknowledgments

The work is supported by the Australian Antarctic Science Program (Project 4528). N T is funded by an Australian Government Research Training Program Scholarship administered by the University of Adelaide. L G B is supported by the Australian Research Council (FT190100404, DP200102828). P R was supported by the Australian Bureau of Meteorology, R M by the Australian Antarctic Division, and both by the Australian Government's Australian Antarctic Partnership Program. This study contributes to the Australian Centre for Excellence in Antarctic Science. We would like to acknowledge the NSIDC, CSIRO and BoM for making both the sea ice concentration and ocean hindcast data freely available. We want to thank the two anonymous reviewers for providing constructive comments which helped improve this paper and the editor for handling it.

ORCID iDs

N J Teder https://orcid.org/0000-0001-6058-4317
L G Bennetts https://orcid.org/0000-0001-9386-7882
R A Massom https://orcid.org/0000-0003-1533-5084

References

[1] Bindschadler R *et al* 2011 Getting around Antarctica: new high-resolution mappings of the grounded and freely-floating boundaries of the Antarctic ice sheet created for the International polar year *Cryosphere* **5** 569–88
[2] IPCC 2021 Summary for policymakers *Climate Change 2021: The Physical Science Basis. Contribution of Working Group I to the Sixth Assessment Report of the Intergovernmental Panel on Climate Change* (Cambridge: Cambridge University Press) (Accepted)
[3] Lipscomb W H, Leguy G R, Jourdain N C, Asay-Davis X, Seroussi H and Nowicki S 2021 ISMIP6-based projections of ocean-forced Antarctic ice sheet evolution using the community ice sheet model *Cryosphere* **15** 633–61
[4] Dupont T K and Alley R B 2005 Assessment of the importance of ice-shelf buttressing to ice-sheet flow *Geophys. Res. Lett.* **32** L04503
[5] Gudmundsson G H 2013 Ice-shelf buttressing and the stability of marine ice sheets *Cryosphere* **7** 647–55
[6] DeConto R M and Pollard D 2016 Contribution of Antarctica to past and future sea-level rise *Nature* **531** 591–7
[7] Meredith M *et al* 2019 Chapter 3: polar regions *IPCC Special Report on the Ocean and Cryosphere in a Changing Climate* (Cambridge: Cambridge University Press)
[8] DeConto R M *et al* 2021 The Paris Climate Agreement and future sea-level rise from Antarctica *Nature* **593** 83–89
[9] Pritchard H D, Ligtenberg S R M, Fricker H A, Vaughan D G, Van Den Broeke M R and Padman L 2012 Antarctic ice-sheet loss driven by basal melting of ice shelves *Nature* **484** 502–5
[10] Rignot E, Mouginot J, Scheuchl B, Van Den Broeke M, Van Wessem M J and Morlighem M 2019 Four decades of Antarctic ice sheet mass balance from 1979–2017 *Proc. Natl Acad. Sci. USA* **116** 1095–103
[11] Pattyn F and Morlighem M 2020 The uncertain future of the Antarctic ice sheet *Science* **367** 1331–5
[12] Rott H, Skvarca P and Nagler T 1996 Rapid collapse of northern Larsen ice shelf, Antarctica *Science* **271** 788–92
[13] Rack W and Rott H 2004 Pattern of retreat and disintegration of the Larsen B ice shelf, Antarctic Peninsula *Ann. Glaciol.* **39** 505–10
[14] Scambos T A, Bohlander J A, Shuman C A and Skvarca P 2004 Glacier acceleration and thinning after ice shelf collapse in the Larsen B embayment, Antarctica *Geophys. Res. Lett.* **31** L18402
[15] Rignot E, Casassa G, Gogineni P, Krabill W, Rivera A and Thomas R 2004 Accelerated ice discharge from the Antarctic Peninsula following the collapse of Larsen B iceshelf *Geophys. Res. Lett.* **31** 2–5
[16] Braun M and Humbert A 2009 Recent retreat of Wilkins ice shelf reveals new insights in ice shelf breakup mechanisms *IEEE Geosci. Remote Sens. Lett.* **6** 263–7
[17] Skvarca P, Rack W, Rott H and Donángelo T I Y 1998 Evidence of recent climatic warming on the eastern Antarctic Peninsula *Ann. Glaciol.* **27** 628–32
[18] Scambos T, Hulbe C and Fahnestock M 2003 Climate-induced ice shelf disintegration in the Antarctic Peninsula *Antarctic Peninsula Climate Variability: Historical and Paleoenvironmental Perspectives* (Antarctic Research Series vol 79) (Washington, DC: American Geophysical Union) pp 79–92
[19] Stammerjohn S, Massom R, Rind D and Martinson D 2012 Regions of rapid sea ice change: an inter-hemispheric seasonal comparison *Geophys. Res. Lett.* **39** L06501
[20] Parkinson C L 2019 A 40-y record reveals gradual Antarctic sea ice increases followed by decreases at rates far exceeding the rates seen in the Arctic *Proc. Natl Acad. Sci. USA* **116** 14414–23
[21] De Santis A, Maier E, Gomez R and Gonzalez I 2017 Antarctica, 1979–2016 sea ice extent: total versus regional trends, anomalies and correlation with climatological variables *Int. J. Remote Sens.* **38** 7566–84
[22] Eayrs C, Li X, Raphael M N and Holland D M 2021 Rapid decline in Antarctic sea ice in recent years hints at future change *Nat. Geosci.* **14** 460–4
[23] Shu Q, Wang Q, Song Z, Qiao F, Zhao J, Chu M and Li X 2020 Assessment of sea ice extent in CMIP6 With comparison to observations and CMIP5 *Geophys. Res. Lett.* **47** e2020GL087965

[24] Turner J, Harangozo S A, Marshall G J, King J C and Colwell S R 2002 Anomalous atmospheric circulation over the Weddell Sea, Antarctica during the Austral summer of 2001/02 resulting in extreme sea ice conditions *Geophys. Res. Lett.* **29** 2–5
[25] Massom R A, Scambos T A, Bennetts L G, Reid P, Squire V A and Stammerjohn S E 2018 Antarctic ice shelf disintegration triggered by sea ice loss and ocean swell *Nature* **558** 383–9
[26] Bennetts L G, Peter M A, Squire V A and Meylan M H 2010 A three-dimensional model of wave attenuation in the marginal ice zone *J. Geophys. Res. Oceans* **115** F02015
[27] Glasser N F and Scambos T A 2008 A structural glaciological analysis of the 2002 Larsen B ice-shelf collapse *J. Glaciol.* **54** 3–16
[28] Rignot E, Jacobs S, Mouginot J and Scheuchl B 2013 Ice-shelf melting around Antarctica *Science* **341** 266–70
[29] Banwell A F, Willis I C, Macdonald G J, Goodsell B and MacAyeal D R 2019 Direct measurements of ice-shelf flexure caused by surface meltwater ponding and drainage *Nat. Commun.* **10** 730
[30] Lipovsky B P 2020 Ice shelf rift propagation: stability, three-dimensional effects and the role of marginal weakening *Cryosphere* **14** 1673–83
[31] Cathles L M I V, Okal E A and MacAyeal D R 2009 Seismic observations of sea swell on the floating Ross Ice Shelf, Antarctica *J. Geophys. Res. Earth Surf.* **114** F02015
[32] Bromirski P D, Diez A, Gerstoft P, Stephen R A, Bolmer T, Wiens D A, Aster R C and Nyblade A 2015 Ross ice shelf vibrations *Geophys. Res. Lett.* **42** 7589–97
[33] Holdsworth G and Glynn J 1978 Iceberg calving from floating glaciers by a vibrating mechanism *Nature* **274** 464–6
[34] Brunt K M, Okal E A and Macayeal D R 2011 Antarctic ice-shelf calving triggered by the Honshu (Japan) earthquake and tsunami, March 2011 *J. Glaciol.* **57** 785–8
[35] Bromirski P D, Chen Z, Stephen R A, Gerstoft P, Arcas D, Diez A, Aster R C, Wiens D A and Nyblade A 2017 Tsunami and infragravity waves impacting Antarctic ice shelves *J. Geophys. Res. Oceans* **122** 5786–801
[36] Bennetts L G and Squire V A 2012 On the calculation of an attenuation coefficient for transects of ice-covered ocean *Proc. R. Soc.* A **468** 136–62
[37] Fox C and Squire V 1991 Coupling between the ocean and an ice shelf *Ann. Glaciol.* **15** 101–8
[38] Bennetts L G and Meylan M H 2021 Complex resonant ice shelf vibrations *SIAM J. Appl. Math.* **81** 1483–502
[39] MacAyeal D R *et al* 2006 Transoceanic wave propagation links iceberg calving margins of Antarctica with storms in tropics and Northern Hemisphere *Geophys. Res. Lett.* **33** 2–5
[40] Chen Z *et al* 2019 Ross Ice Shelf icequakes associated with ocean gravity wave activity *Geophys. Res. Lett.* **46** 8893–902
[41] Young I R, Zieger S and Babanin A V 2011 Global trends in wind speed and wave height *Science* **332** 451–5
[42] Meylan M H, Ilyas M, Lamichhane B P and Bennetts L G 2021 Swell-induced flexural vibrations of a thickening ice shelf over a shoaling seabed *Proc. R. Soc.* A **477** 20210173
[43] Reid P A and Massom R A 2022 Change and variability in Antarctic coastal exposure, 1979–2020 *Nat. Commun.* **13** 1–11
[44] Greene C A, Young D A, Gwyther D E, Galton-Fenzi B K and Blankenship D D 2018 Seasonal dynamics of Totten Ice Shelf controlled by sea ice buttressing *Cryosphere* **12** 2869–82
[45] Miles B, Stokes C and Jamieson S 2018 Velocity increases at Cook Glacier, East Antarctica, linked to ice shelf loss and a subglacial flood event *Cryosphere* **12** 3123–36
[46] Cavalieri D J, Parkinson C L, Gloersen P and Zwally H 1996 *Sea Ice Concentrations from Nimbus-7 SMMR and DMSP SSM/I-SSMIS Passive Microwave Data* (Boulder, CO: Digital Media)
[47] Greene C A, Gwyther D E and Blankenship D D 2017 Antarctic Mapping Tools for MATLAB *Comput. Geosci.* **104** 151–7
[48] Smith G A, Hemer M, Greenslade D, Trenham C, Zieger S and Durrant T 2020 Global wave hindcast with Australian and Pacific Island Focus: from past to present *Geosci. Data J.* **00** 1–10
[49] Chawla A, Spindler D and Tolman H L 2011 A thirty year wave hindcast using the latest NCEP climate forecast system reanalysis winds *Int. Workshop on Wave Hindcasting and Forecasting* pp 1–11
[50] Tolman H L 2003 Treatment of unresolved islands and ice in wind wave models *Ocean Model.* **5** 219–31
[51] The WAVEWATCH III R Development Group (WW3DG) 2016 User manual and system documentation of WAVEWATCH III R version 5.16 *Technical Note* 329 (College Park, MD: NOAA/NWS/NCEP/MMAB) p 326
[52] Comiso J C and Nishio F 2008 Trends in the sea ice cover using enhanced and compatible AMSR-E, SSM/ I and SMMR data *J. Geophys. Res. Oceans* **113** C02S07
[53] Eayrs C, Holland D, Francis D, Wagner T, Kumar R and Li X 2019 Understanding the seasonal cycle of Antarctic sea ice extent in the context of longer-term variability *Rev. Geophys.* **57** 1037–64
[54] Gwyther D E, Galton-Fenzi B K, Hunter J R and Roberts J L 2014 Simulated melt rates for the Totten and Dalton ice shelves *Ocean Sci.* **10** 267–79
[55] Mayet C, Testut L, Legresy B, Lescarmontier L and Lyard F 2013 High-resolution barotropic modeling and the calving of the Mertz Glacier, East Antarctica *J. Geophys. Res. Oceans* **118** 5267–79
[56] Massom R A, Hill K L, Lytle V I, Worby A P, Paget M J and Allison I 2001 Effects of regional fast-ice and iceberg distributions on the behaviour of the Mertz Glacier polynya, East Antarctica *Ann. Glaciol.* **33** 391–8
[57] Tamura T, Williams G D, Fraser A D and Ohshima K I 2012 Potential regime shift in decreased sea ice production after the Mertz Glacier calving *Nat. Commun.* **3** 826
[58] Cougnon E A, Galton-Fenzi B K, Rintoul S R, Legrésy B, Williams G D, Fraser A D and Hunter J R 2017 Regional changes in icescape impact shelf circulation and basal melting *Geophys. Res. Lett.* **44** 11519–27
[59] Comiso J C, Kwok R, Martin S and Gordon A L 2011 Variability and trends in sea ice extent and ice production in the Ross Sea *J. Geophys. Res. Oceans* **116** C04021
[60] Arrigo K R and van Dijken G L 2003 Impact of iceberg C-19 on Ross Sea primary production *Geophys. Res. Lett.* **30** 1–4
[61] Criscitiello A S, Das S B, Evans M J, Frey K E, Conway H, Joughin I, Medley B and Steig E J 2013 Ice sheet record of recent sea-ice behavior and polynya variability in the Amundsen Sea, West Antarctica *J. Geophys. Res. Oceans* **118** 118–30
[62] Miles B W J, Stokes C R, Jenkins A, Jordan J R, Jamieson S S R and Gudmundsson G H 2020 Intermittent structural weakening and acceleration of the Thwaites Glacier Tongue between 2000 and 2018 *J. Glaciol.* **66** 485–95
[63] Kwok R, Pang S S and Kacimi S 2017 Sea ice drift in the Southern Ocean: regional patterns, variability and trends *Elementa* **5** 1–16
[64] Morim J *et al* 2021 Global-scale changes to extreme ocean wave events due to anthropogenic warming *Environ. Res. Lett.* **16** 1–9
[65] Humbert A and Braun M 2008 The Wilkins Ice Shelf, Antarctica: break-up along failure zones *J. Glaciol.* **54** 943–4
[66] Meier W N, Fetterer F, Windnagel A K and Stewart J S 2021 *NOAA/NSIDC Climate Data Record of Passive Microwave Sea Ice Concentration, Version 4*
[67] Hersbach H *et al* 2019 Global reanalysis: goodbye ERA-Interim, hello ERA5 *ECMWF Newsl.* **159** 17–24
[68] Zhao X, Su H, Stein A and Pang X 2015 Comparison between AMSR-E ASI sea-ice concentration product, MODIS and pseudo-ship observations of the Antarctic sea-ice edge *Ann. Glaciol.* **56** 45–52

[69] Roach L A et al 5 2020 Antarctic sea ice area in CMIP6 Geophys. Res. Lett. 47 e2019GL086729
[70] Notz D and SIMIP Community 2020 Arctic sea ice in CMIP6 Geophys. Res. Lett. 47 1–11
[71] Casas-Prat M, Wang X L and Swart N 2018 CMIP5-based global wave climate projections including the entire arctic ocean Ocean Model. 123 66–85
[72] Morim J et al 2019 Robustness and uncertainties in global multivariate wind-wave climate projections Nat. Clim. Change 9 711–8
[73] Bennetts L G, O'Farrell S and Uotila P 2017 Impacts of ocean-wave-induced breakup of Antarctic sea ice via thermodynamics in a stand-alone version of the CICE sea-ice model Cryosphere 11 1035–40
[74] Boutin G, Lique C, Ardhuin F, Rousset C, Talandier C, Accensi M and Girard-Ardhuin F 2020 Towards a coupled model to investigate wave-sea ice interactions in the Arctic marginal ice zone Cryosphere 14 709–35